Rare Metal Materials and Engineering
Volume 53, Issue 10, October 2024
Available online at www.rmme.ac.cn

Science Press

Cite this article as: Li Hui, Chen Geng, Zhang Sheng, et al. Preparation of High-Entropy Alloy-Ceramic Coating Composites on Steel Surfaces by Combined Process and Their Mechanical Properties[J]. Rare Metal Materials and Engineering, 2024, 53(10): 2735-2746. DOI: 10.12442/j.issn.1002-185X.E20240311.

ARTICLE

Preparation of High-Entropy Alloy-Ceramic Coating Composites on Steel Surfaces by Combined Process and Their Mechanical Properties

Li Hui[1], Chen Geng[1], Zhang Sheng[1], Liang Jinglong[1], Huo Dongxing[2], Yang Yu[3]

[1] Key Laboratory of Modern Metallurgy Technology, Ministry of Education, College of Metallurgy and Energy, North China University of Science and Technology, Tangshan 063210, China; [2] School of Mechanical Engineering, North China University of Technology, Tangshan 063210, China; [3] Comprehensive Testing and Analyzing Center, North China University of Science and Technology, Tangshan 063210, China

Abstract: A combined process of molten salt electro-deoxidation and vacuum hot-pressing sintering was proposed to prepare AlCrFeNiTi$_x$ high-entropy alloy (HEA)-TiN ceramic coating composites on low-carbon steel surfaces, where nitrides were introduced from BN isolater between graphite mold and HEA powders. The effect of Ti content on the microstructure, ultimate tensile strength, hardness, and wear resistance of the composites was investigated, and the bonding mechanism was elucidated. Results demonstrate that the composites have excellent hardness and wear resistance. The hardness of composites is significantly increased with the increase in Ti content. The extremely high wear resistance is attributed to the extremely high melting point and high thermal hardness of TiN, which can effectively prevent oxidation deformation of the worn surface.

Key words: high-entropy alloy; ceramic coating composites; molten salt electro-deoxidization; vacuum hot-pressing sintering; mechanical properties

Traditional single materials cannot satisfy the performance requirements in specialized fields, such as aerospace, marine, rail transportation, naval vessels, vehicles, and nuclear power[1–3]. Taking mechanical components as an example, approximately 80% component failures are caused by wear, and around 30% energy is wasted due to friction[4–5]. Surface coating modification is one of the common methods to improve material properties, which leads to low energy consumption, low maintenance cost, and particularly less production accidents[6–7].

Low-carbon steel is a widely used material in iron and steel materials. Coating composites with low cost can retain excellent properties on the low-carbon steel surfaces, such as good corrosion resistance, fine wear resistance, and superb oxidation resistance[8]. Recently, high-entropy alloys (HEAs) have attracted much attention as the coating composite material due to their excellent properties, such as high strength, high toughness, excellent wear resistance, and outstanding oxidation and corrosion resistance[9–13]. The low-cost and short-period preparation process of HEA coating is crucial for overall performance enhancement of low-carbon steel substrates.

Currently, the traditional preparation techniques of surface composites include electroplating[14], thermal spraying[15], hard facing[16], laser cladding[17], physical vapor deposition[18–19], and chemical vapor deposition[20–21]. Coatings prepared by laser cladding have high bonding ability but uneven thickness[22]. Vapor phase deposition is generally used for dielectrics, semiconductors, conductors, and other functional thin film composite, which does not apply to the preparation of coating composite on the steel materials. Moreover, the abovementioned processes require high temperature treatment, which will cause environment pollution to a certain extent. Therefore, the preparation process with characteristics of low

Received date: May 24, 2024
Foundation item: National Natural Science Foundation of China (52174315); Youth Scholars Promotion Plan of North China University of Science and Technology (QNTJ202304)
Corresponding author: Yang Yu, Ph. D., Comprehensive Testing and Analyzing Center, North China University of Science and Technology, Tangshan 063210, P. R. China, Tel: 0086-315-8816212, E-mail: yyu@ncst.edu.cn

temperature, short period, and environmental friendliness for coating composites has attracted wide concern[23–33].

In this research, $AlCrFeNiTi_x$ HEA-ceramic coating composites were prepared on the low-carbon steel by a combined process (molten salt electro-deoxidization and vacuum hot-pressing sintering process). Initially, the $AlCrFeNiTi_x$ HEA powder was prepared by molten salt electro-deoxidization, namely FFC process. Then, HEA-ceramic coating composites (carbon steel as the substrate and coated HEA powder as the composites) were prepared through vacuum hot-pressing sintering (VHPS). The effect of Ti content on the crystal structure, microstructure, ultimate tensile strength, hardness, and wear resistance of the composites was investigated, and the bonding mechanism between carbon steel matrix and coating was elucidated in this research.

1 Experiment

Al_2O_3, Cr_2O_3, Fe_2O_3, NiO, and TiO_2 were used as mixed oxide source materials. The mass of each oxide was calculated based on the alloy composition with different Ti contents. The total mass of the mixed oxides was 4 g. The mixed oxides were then encapsulated in stainless steel mesh based on the atomic ratios.

The experiment employed a graphite crucible as the anode and a mixture of oxide precursors as the cathode to improve the reaction rate, as shown in Fig.1. Initially, 200 g $CaCl_2$ was placed in the graphite crucible and dried at 573 K for 12 h. Subsequently, a nickel plate and the graphite crucible were immersed in the molten salt as the cathode and anode, respectively, under the condition of continuous argon flow throughout the process. A constant voltage of 2.8 V was applied to the system for pre-electrolysis, which was halted once the current-time curve was stabilized without further fluctuations. Then, the nickel plate as the cathode was replaced with the mixture of oxide precursors. Electrolysis was then conducted under the constant voltage of 3.1 V for 24 h. After the electro-deoxidation, the cathode of stainless steel mesh was raised to the surface of the molten salt. Continuous argon flow was maintained throughout the cooling process to prevent the product oxidation. After cooling process, the cathode was removed, cleaned by ultrasound treatment in deionized water, and subsequently vacuum-dried at 333 K for 3 h.

The cathode product was ground and sieved to obtain fine particles after vacuum drying. Initially, 15 g low-carbon steel powder was placed in a graphite mold. Then, 0.5 g electro-deoxidized product was evenly spread onto the surface of low-carbon steel. Adding BN isolator between the mold and the product as the nitrogen source of the composites can also effectively alleviate the separation of different parts during the release process. Then, the as-prepared graphite mold was then placed inside a vacuum sintering furnace. The pressure inside the vacuum sintering furnace could reach 30 MPa after three times of vacuum evacuation and argon gas injection processes. Sintering process was conducted at 1373 K under specific pressure conditions for 1 h. After the sintering treatment, the graphite mold and the product were removed together with the cooling furnace. The resulting product was the low-carbon steel-HEA-ceramic coating composites. The schematic diagrams of VHPS apparatus and the composites are shown in Fig.2.

The test samples underwent mild grinding and polishing to investigate the microstructure. The room-temperature strength of HEAs was tested using the WDW-100 electronic universal testing machine. The tensile strain rate was set as 1×10^{-4} m/s. Before experiment, the surfaces of the I-shaped samples were sanded with 600#–3000# sandpaper to ensure that there were no visible scratches on the sample surfaces. Each sample was tested three times to ensure the result accuracy. Hardness was measured using the Model HV-115 Vickers hardness tester produced by Kanagawa, Japan. The friction and wear testing machine (TRM1000, WAZUA, Germany) was used for the study of wear behavior under dry sliding conditions. Cylindrical wear samples with dimension of Φ10 mm×3 mm were fixed on the support and rubbed against a SKH51 high-speed steel disk with diameter of 100 cm, which was served as the friction counterpart. The distance between the wear sample and the disk center was set as 20 mm. The load was 29.4 N and the sliding speed was 0.8 m/s during the friction and wear experiments. The sliding distance was determined based on the alloy composition as 500–3000 m.

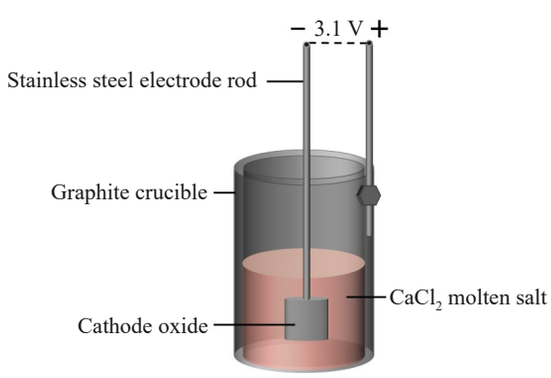

Fig.1 Schematic diagram of molten salt electro-deoxidation equipment

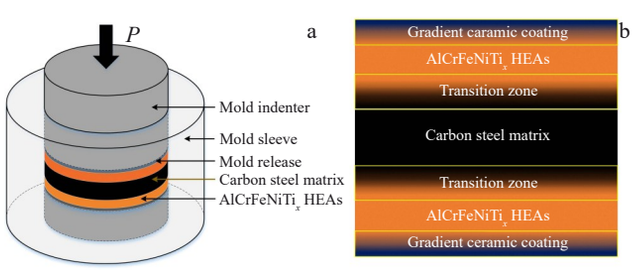

Fig.2 Schematic diagrams of VHPS preparation process (a) and structure (b) of low-carbon steel-HEA-ceramic coating composites

Crystal structure was determined using D/max 2500PC X-ray diffractometer (XRD) manufactured by Rigaku, Japan. Elemental analysis and content were determined using ICAP6300 DUO inductively coupled plasma emission spectrometer produced by ThermoFisher Scientific. Sample morphology and microstructure were observed using scanning electron microscope (SEM, TESCAN VEGA II with Oxford INCA Energy 350 tungsten filament and ThermoFisher Scientific Quattro S). SEM was equipped with energy-dispersive X-ray spectroscope (EDS) and backscattered electron (BSE) mode was employed. The micro-area chemical composition of the composites was analyzed using JXA-8530F Plus filed emission-electro-probe microanalyzer (FE-EPMA) produced by JEOL, and qualitative and quantitative analyses of the elements were conducted.

2 Results and Discussion

2.1 HEA powder prepared by FFC process

Fig. 3 shows XRD patterns of the electro-deoxidation products of HEA powder with different Ti contents, where specific body-centered cubic (bcc) structures can be observed. Both ordered bcc1 and disordered bcc2 structures of $AlCrFeNiTi_x$ HEAs can be observed in the electro-deoxidation products with different Ti contents. The ordered and disordered phases in these alloys are identified as $AlNi_2Ti$ B2 phase and CrFe A2 phase, respectively. In addition to bcc phase, TiC phase can also be observed in $AlCrFeNiTi_x$ HEA when x=0.5. Fe_2Ti phase appears when x=1.5, which is attributed to the element ratio and the low-temperature reduction conditions of the molten salt electro-deoxidation process. Excess Ti reacts with the reduced Fe at the cathode, forming the Fe_2Ti binary alloy. Table 1 shows the chemical composition of the electro-deoxidation cathode products of $AlCrFeNiTi_x$ HEAs. The results indicate that the element composition of the product powder is consistent with that of sample before electro-deoxidation. All cathode oxides are fully reduced during the molten salt electro-deoxidation process with no significant dissolution loss in the product.

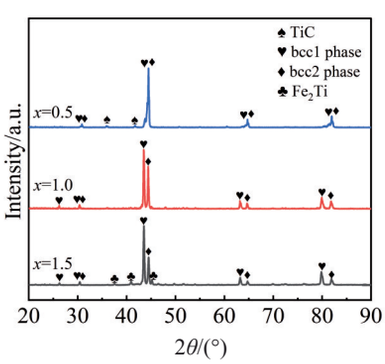

Fig.3 XRD patterns of $AlCrFeNiTi_x$ HEA powders with different Ti contents

Table 1 Chemical composition of electro-deoxidation cathode products of $AlCrFeNiTi_x$ HEAs (at%)

x	Al	Cr	Fe	Ni	Ti
0.5	0.25	0.22	0.23	0.20	0.10
1.0	0.23	0.19	0.21	0.18	0.19
1.5	0.17	0.17	0.21	0.18	0.27

Fig. 4 shows SEM-EDS analysis results of $AlCrFeNiTi_x$ HEA powders. The electro-deoxidation product becomes clustered aggregates, which are composed of nodular particles. The increase in Ti content leads to the significant reduction in particle size of the electro-deoxidation product. The melting point of the alloy is increased and the sintering growth between particles is weakened with the Ti addition, resulting in the obvious decrease in grain size from 4–6 μm (x=0.5) to 2 μm (x=1.5). EDS analysis results indicate that the distributions of elements in the particle products are relatively uniform.

2.2 Composites prepared by VHPS

Fig. 5 displays XRD patterns of $AlCrFeNiTi_x$-TiN coating composites with different Ti contents. The ordered B2 phase and disordered A2 phase are both present in the composites with different Ti contents, resulting in the formation of $AlCrFeNiTi_x$ HEAs with bcc structure. Consistent with the HEA powder, the ordered and disordered phases in the composites are $AlNi_2Ti$ B2 phase and CrFe A2 phase, respectively. $AlCoCrFeNi_x$-TiN composites primarily consist of CrFeCo-type solid solution with ordered NiAl nanoparticles as precipitates.

In addition to B2 and A2 phases, TiN exists in $AlCoCrFeNi_{0.5}$-TiN coating composite accompanied with the reduction in FeN, demonstrating that Ti reacts more readily with BN to form TiN due to the better stability of TiN, compared with that of FeN. According to FE-EPMA and EDS analysis results in Fig. 6, the Al and Ni elements overlap each other, forming the ordered B2 phase[34–37]. The size of B2 phase (including AlNi) is increased with the increase in Ti content. EDS analysis reveals the overlapping distribution of Ti, N, and C elements, indicating the formation of the second phases (TiN and TiC) as a result of the reactions between Ti and N or C.

A solid solution is formed between Ti and AlNi-rich B2 phase with the increase in Ti content, leading to the shift of diffraction peak angles of $AlNi_2Ti$-type B2 phase[38]. Al, Ni, and Ti elements have similar distributions in $AlCoCrFeNi_{1.0}$-TiN coating composite, as shown in Fig. 6b. The intensity of TiN is gradually increased with the increase in Ti content.

Two kinds of topologically close-packed (TCP) inter-metallic compound phases (σ phase and Cr_3Si-type Ti_3Al phase) appear in $AlCoCrFeNi_{1.5}$-TiN coating composite, as shown in Fig. 6c. With the increase in Ti content, the lattice distortion of the alloy becomes more serious, which eventually leads to the precipitation of the intermetallic compound phases. The intensity of the disordered A2 phase is decreased in $AlCoCrFeNi_{1.5}$-TiN coating composite with the precipitation of σ phase (riched CrFe). N reacts completely with excess Ti, and thus FeN phase in $AlCoCrFeNi_{1.5}$-TiN coating composite

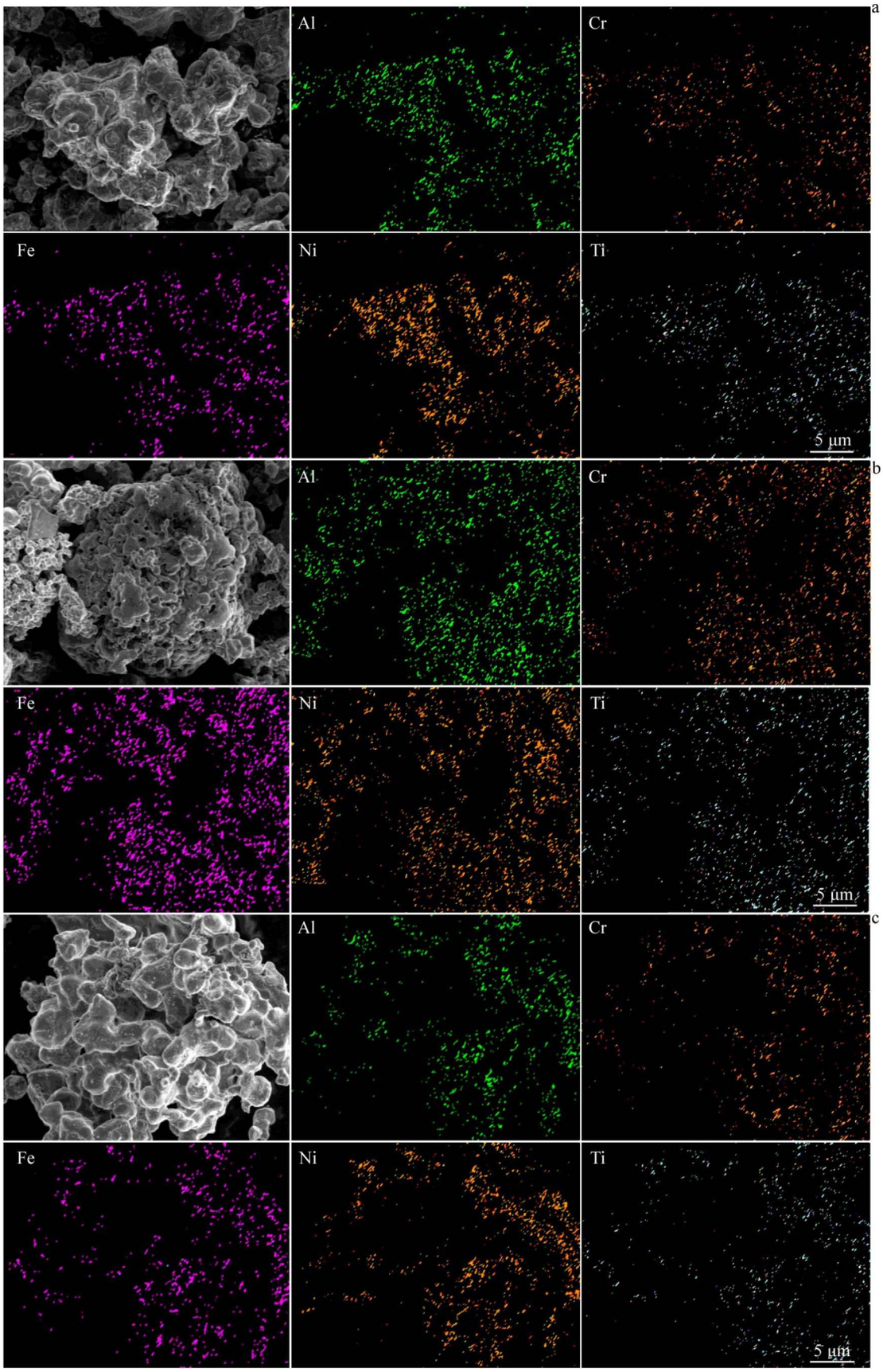

Fig.4 SEM-EDS analysis results of deoxidized AlCrFeNiTi$_x$ HEA powders: (a) x=0.5; (b) x=1.0; (c) x=1.5

disappears with the increase in Ti content. Ti and N elements have overlapping distributions, whereas the distributions of Fe and N elements are not similar.

Fig. 7 displays BSE-EDS analysis results of AlCrFeNiTi$_x$-

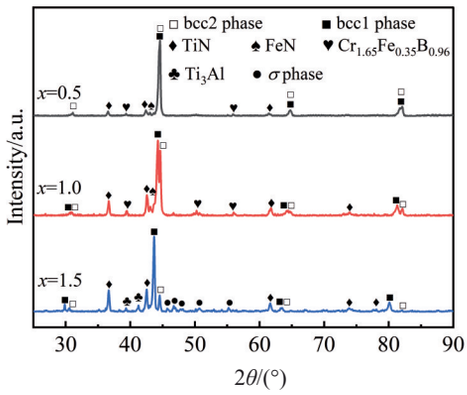

Fig.5 XRD patterns of $AlCrFeNiTi_x$-TiN coating composites with different Ti contents

TiN coating composites with different Ti contents. The phase distribution in $AlCoCrFeNi_{0.5}$-TiN composite is relatively uniform. EDS analysis results confirm that the element distribution is similar to that from the previous FE-EPMA results. When x=1.0 and 1.5, TiN phase segregation is obvious. Phase segregation is caused by the increase in Ti content, leading to the precipitation of TiN and TCP phases, as shown in Fig.5 and Fig.6.

Fig. 8 illustrates the bonding mechanism between coating composites and matrix. The composite has obvious boundaries with the matrix and there is no loose structure inside the composites. The effect of VHPS process is quite obvious. At the interface between the composite and the substrate, the elements are uniformly distributed. When x=0.5, Ni diffusion can be observed, whereas Cr and Ti elements have distinct

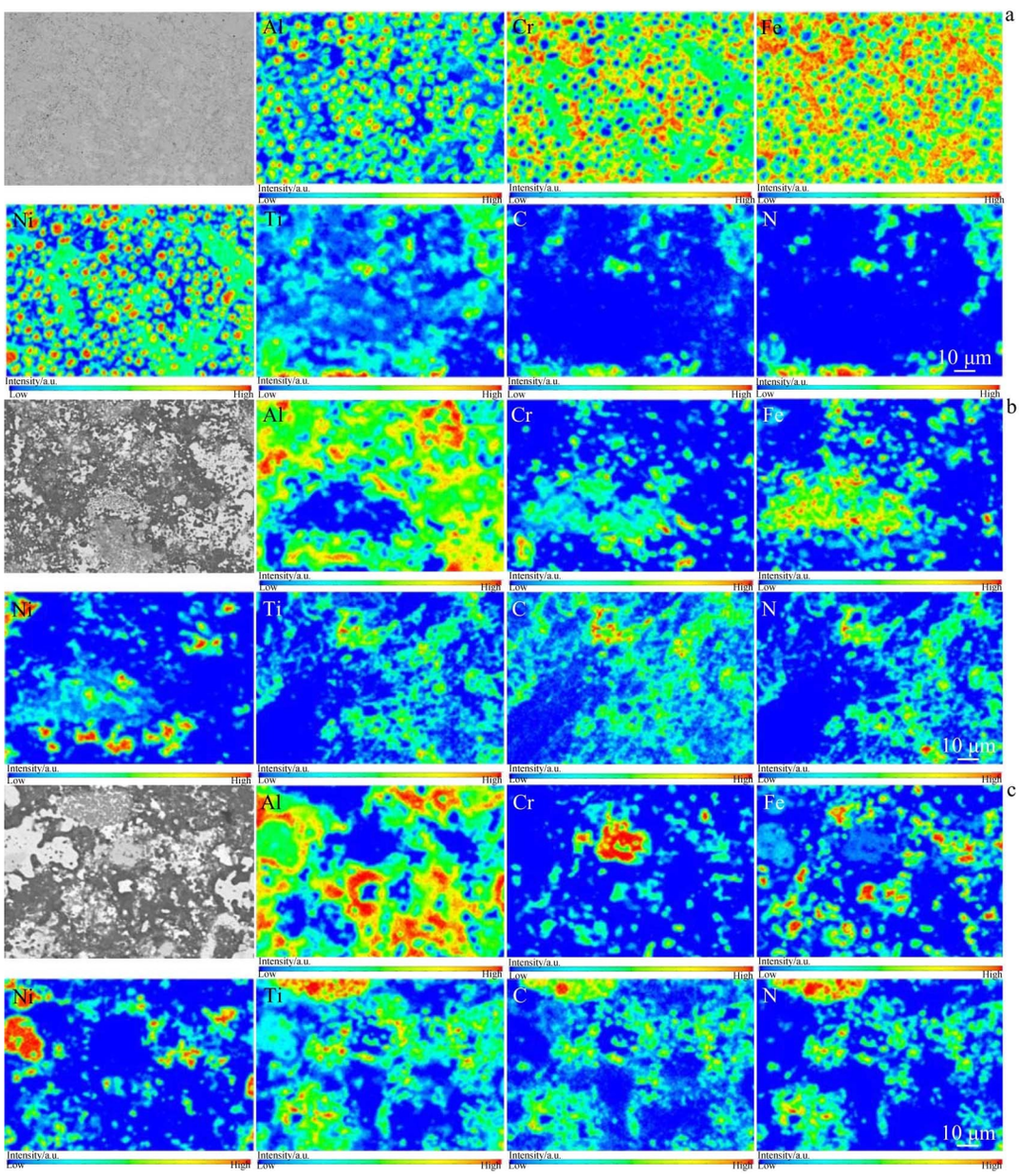

Fig.6 FE-EPMA images and EDS analysis results of $AlCrFeNiTi_x$-TiN coating composites with different Ti contents: (a) x=0.5; (b) x=1.0; (c) x=1.5

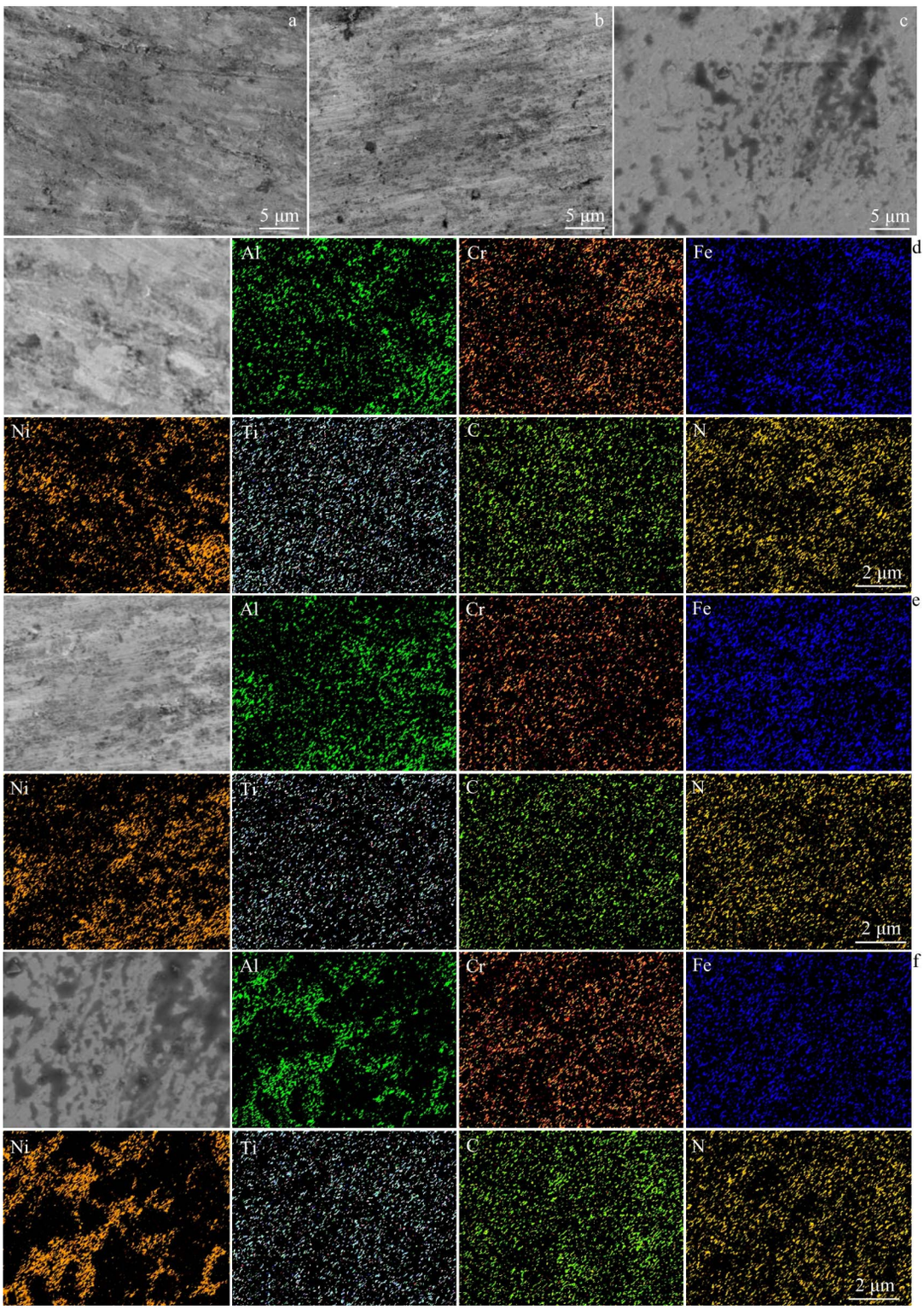

Fig.7 BSE images (a–c) and EDS analysis results (d–f) of AlCrFeNiTi$_x$-TiN coating composites with different Ti contents: (a, d) x=0.5; (b, e) x=1.0; (c, f) x=1.5

boundaries with the Fe element in the substrate. When x=1.0, the metallic Ti in the bonding exhibits distinct boundaries, indicating the restricted diffusion of elements during VHPS process. When x=1.5, Cr and Ti elements begin to slowly diffuse into the substrate, which inhibits the diffusion of Ni into the substrate.

2.3 Mechanical properties

Fig. 9 displays the stress-strain curves of AlCrFeNiTi$_x$-TiN coating composites. Both the tensile strength and ductility of the composites are gradually decreased with the increase in Ti content. The tensile strength decreases from 359 MPa (x=0.5) to 246 MPa (x=1.5) with the increase in Ti content.

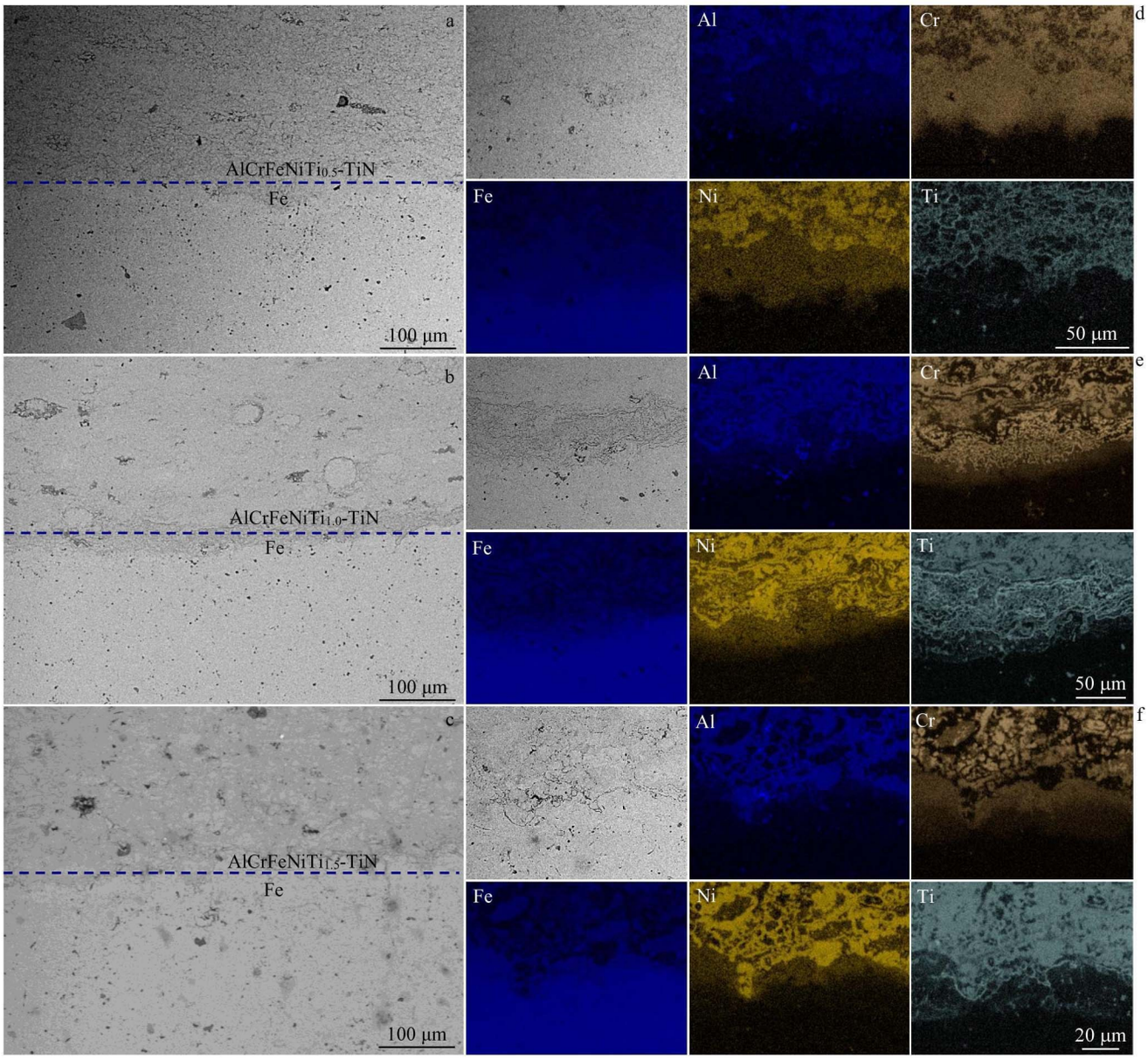

Fig.8 BSE images (a–c) and EDS analysis results (d–f) of cross-sections of AlCrFeNiTi$_x$-TiN coating composites with different Ti contents: (a, d) x=0.5; (b, e) x=1.0; (c, f) x=1.5

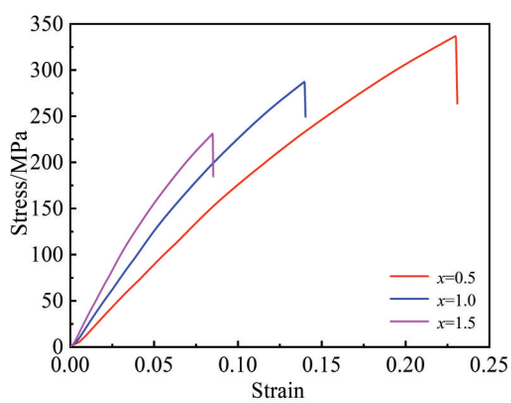

Fig.9 Stress-strain curves of AlCrFeNiTi$_x$-TiN coating composites with different Ti contents

Meanwhile, different composites display poor ductility. XRD analysis shows that the composites consist of B2 and A2 phases. B2 phase offers relatively good strength. Additionally, a large number of FeN particles are generated by the reaction of BN and Fe, which significantly reduces the plasticity of the composites. More and more TiN second phases are generated, which further impairs the plasticity and tensile strength of the composites with the increase in Ti content. Fig. 10 illustrates the fracture surfaces of composites with different Ti contents. Macroscopically, no necking phenomenon can be observed in different composites, and the fracture morphologies show a river-type disintegration, indicating the brittle fracture.

The hardness of AlCrFeNiTi$_x$-TiN coating composites is significantly improved by the precipitation of the second phase (TiN) and intermetallic compounds. Fig. 11 shows the

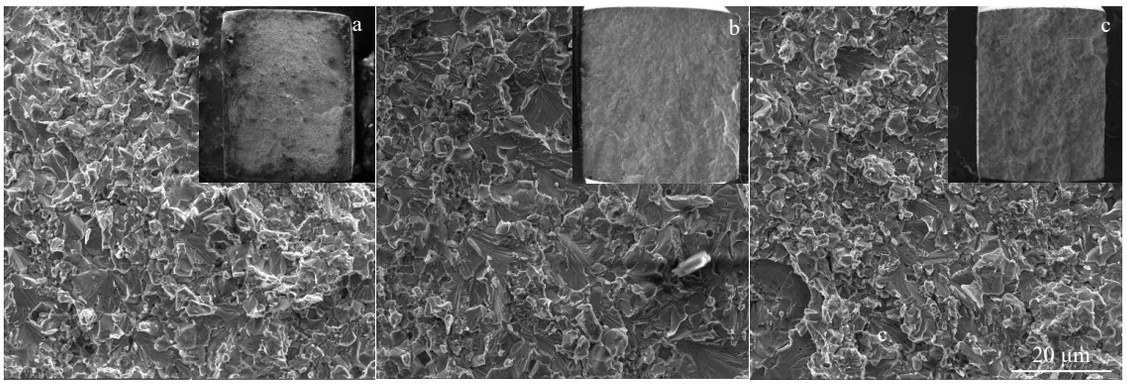

Fig.10 Fracture surface morphologies of AlCrFeNiTi$_x$-TiN coating composites with different Ti contents: (a) x=0.5; (b) x=1.0; (c) x=1.5

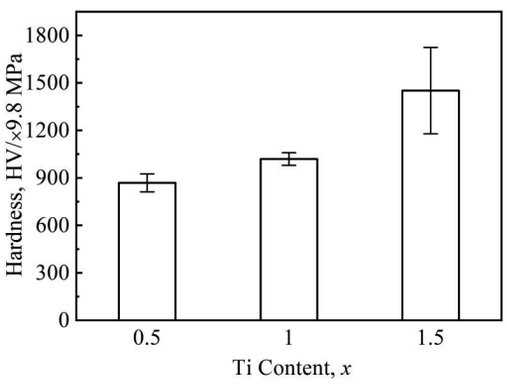

Fig.11 Hardness of AlCrFeNiTi$_x$-TiN coating composites with different Ti contents

hardness of AlCrFeNiTi$_x$-TiN coating composites. It can be seen that the hardness of the composites is increased significantly from 8516 MPa (x=0.5) to 14 220 MPa (x=1.5) with the increase in Ti content. The reasons for the hardness improvement are as follows. Firstly, the second phase (TiN) is precipitated on the surface of AlCrFeNiTi$_{0.5}$-TiN coating composite, which significantly enhances the hardness of the composites, and the amount of TiN is proportional to the Ti content. Secondly, the precipitation of TCP phases (σ phase and Ti_3Al phase) further increases the hardness of composites. TiN, A2, and TCP phases jointly form a ceramic coating on the surface of AlCrFeNiTi$_{1.5}$-TiN coating composite with B2 phase as the matrix, thereby presenting excellent hardness.

The grooves on the wear surfaces of AlCrFeNiTi$_{0.5}$-TiN coating composite are shallower, as shown in Fig. 12. The shape of the wear debris is flake-like and the sizes range from approximately 100 μm to 250 μm, indicating that the adhesive wear mechanism of AlCrFeNiTi$_{0.5}$-TiN coating composite is delamination wear. The wear surface of AlCrFeNiTi$_{0.5}$-TiN coating composite contains a certain amount of oxygen, as listed in Table 2, which indicates that oxidation occurs during friction and deformation. The adhesive wear mechanism can be distinctly reflected by the oxidation wear in addition to delamination wear. Chuang et al[39] found that the flash temperature in the local contact area of the $Al_{0.2}Co_{1.5}CrFeNi_{1.5}$ Ti alloy may exceed 1073 K during dry sliding friction under the conditions of sliding speed of 0.5 m/s and applied load of 29.4 N. Both oxidation and softening phenomena of the alloy become important factors to affect the wear performance at specific temperatures. The degradation in the oxidation wear characteristics of the alloy is attributed to the addition of Ti. According to the oxidation wear mechanism, wear mainly occurs in the real contact area of the surface. EDS analysis results show that the composition of wear debris and friction debris is consistent, indicating that the wear resistance of AlCrFeNiTi$_{0.5}$-TiN coating composite is better than that of high-speed steel.

Only partial peeling occurs on the wear surface of AlCrFeNiTi$_{1.0}$-TiN coating composite. No wear grooves appear, as shown in Fig. 13. The size of flake-shaped debris (ranging from 50 μm to 150 μm) further reduces, indicating that delamination wear is the sole adhesive wear mechanism for AlCrFeNiTi$_{1.0}$-TiN coating composite. The lower oxygen content on the wear surface of AlCrFeNiTi$_{1.0}$-TiN coating composite, as listed in Table 2, further confirms this mechanism. The primary cause of delamination wear is that the surface-removed fragments act as plows during the wear process. Hard fragments can abrade the relatively thin and incompletely coated part, resulting in the formation of periodic delamination fractures on the wear surface. The surface of AlCrFeNiTi$_{1.0}$-TiN composite shows granular morphology. EDS analysis results indicate that the fine granular debris is caused by the high-speed steel friction pair.

The wear surface of AlCrFeNiTi$_{1.5}$-TiN coating composite is smooth and flat, where only local small and shallow pits exist, as shown in Fig. 14. The results in Table 2 indicate that the TiN content is increased with the addition of Ti, leading to the increase in the thickness of TiN coating. The thicker coating effectively prevents oxidation and deformation of the wear surface. Additionally, the precipitation of intermetallic compounds (σ phase and Ti_3Al phase) significantly contributes to the improvement in wear resistance. Both the debris morphology and EDS analysis result suggest that the particle size of AlCrFeNiTi$_{1.5}$-TiN coating composite is less than 1 μm, and its wear resistance is similar to that of AlCrFeNiTi$_{1.0}$-TiN coating composite.

Khrushchev et al[40] pointed out that the wear resistance is

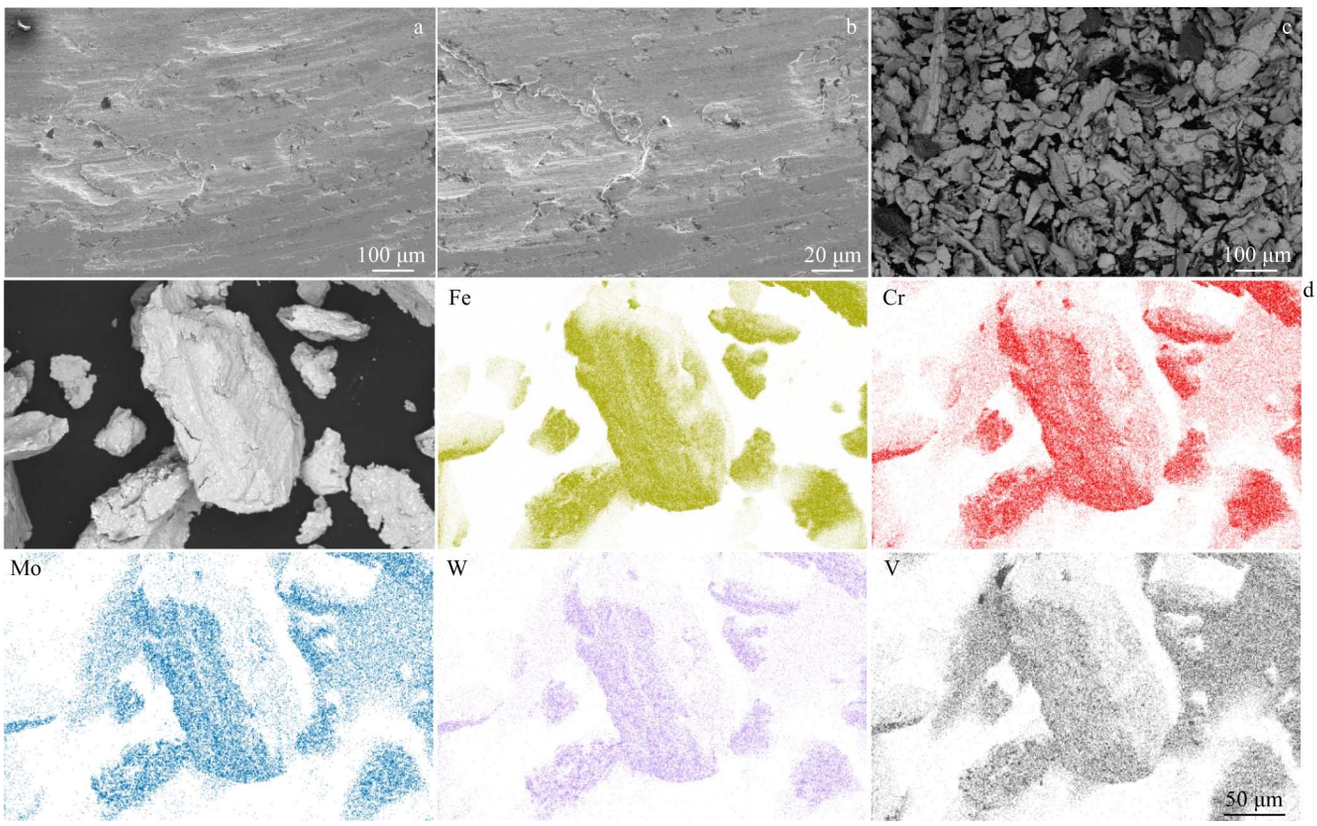

Fig.12 Surface morphologies of AlCrFeNiTi$_{0.5}$-TiN coating composite (a–c); EDS analysis results of wear debris on AlCrFeNiTi$_{0.5}$-TiN coating composite (d)

Table 2 Composition of wear surface of AlCrFeNiTi$_x$-TiN coating composites with different Ti contents (at%)

x	Al	Cr	Fe	Ni	Ti	N	O
0.5	17.45	16.37	17.34	15.92	7.68	17.49	7.75
1.0	16.12	14.48	14.67	16.29	16.05	19.57	2.82
1.5	15.22	13.39	14.10	13.68	21.82	19.73	2.06

directly proportional to the Vickers hardness. Increasing the Ti content in HEAs leads to a significant increase in surface hardness. Ti content in AlCrFeNiTi$_x$ HEAs has a significant impact on the morphology of the wear surface. The surface roughness and deformation degree of composites are decreased noticeably with the increase in Ti content, as shown in Fig.12–Fig.14.

Fig.15 represents the variation curves of the coefficient of friction with sliding distance of AlCrFeNiTi$_x$-TiN coating composites with different Ti contents. The coefficient of friction firstly increases, reaching a peak value, and gradually decreases to a stable state in typical wear tests[41]. Significant

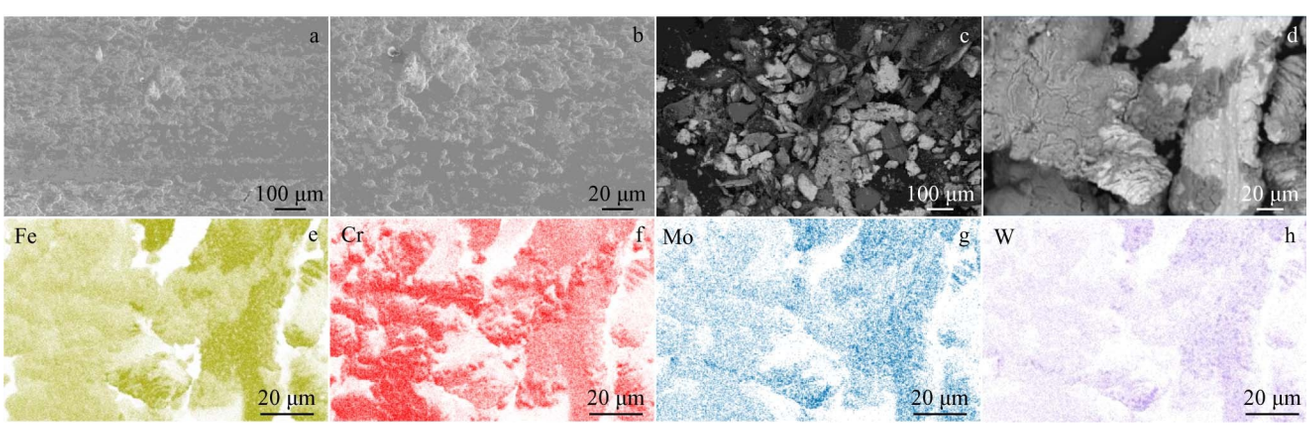

Fig.13 Surface (a–b) and wear debris (c–d) morphologies of AlCrFeNiTi$_{1.0}$-TiN coating composite; EDS element distributions of Fe (e), Cr (f), Mo (g), and W (h) of Fig.13d

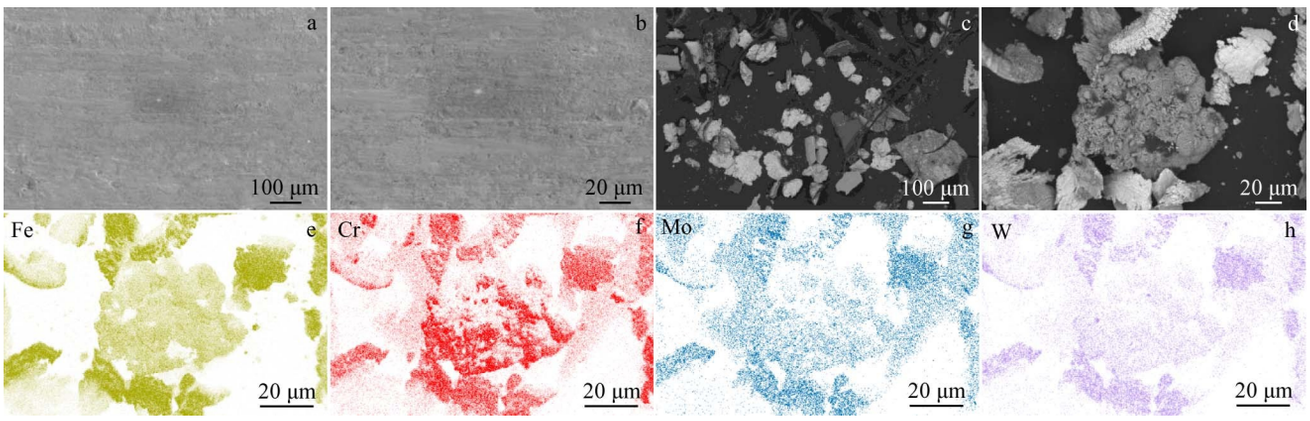

Fig.14 Surface (a–b) and wear debris (c–d) morphologies of AlCrFeNiTi$_{1.5}$-TiN coating composite; EDS element distributions of Fe (e), Cr (f), Mo (g), and W (h) of Fig.14d

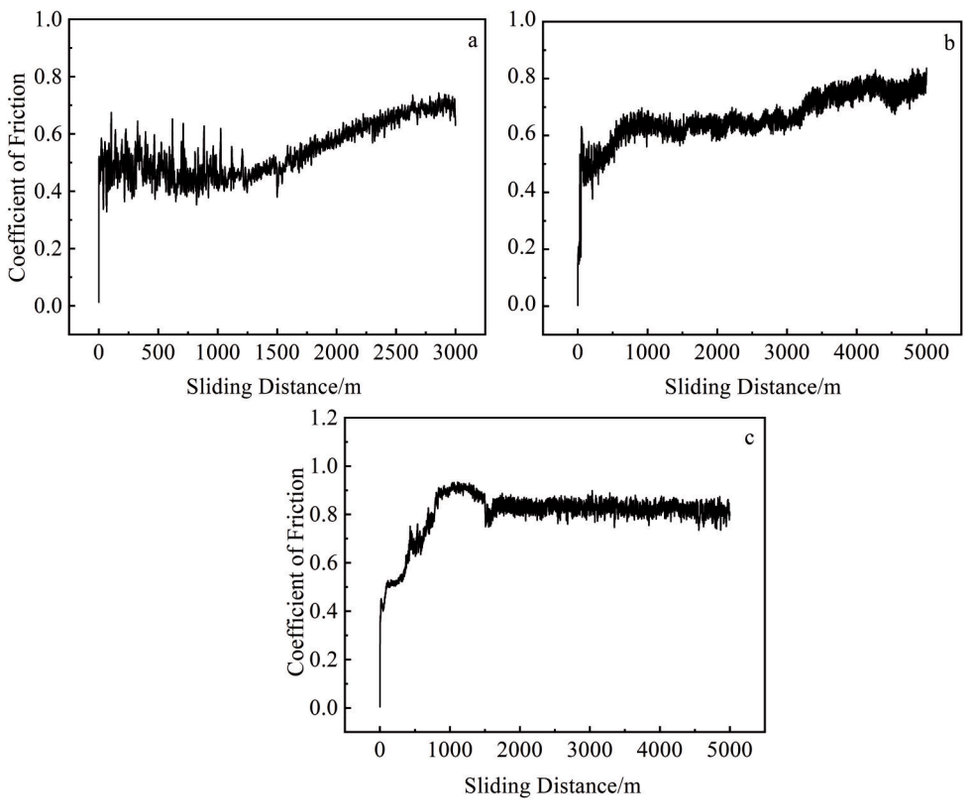

Fig.15 Variation curves of coefficient of friction with sliding distance of AlCrFeNiTi$_x$-TiN coating composites with different Ti contents: (a) x=0.5; (b) x=1.0; (c) x=1.5

fluctuation can be observed in the curves of coefficient of friction of AlCrFeNiTi$_x$-TiN coating composites with different Ti contents. The main reason for this fluctuation is the periodic local fractures on the wear surface caused by delamination wear behavior. Additionally, the coefficient of friction is increased with the accumulation of abrasive particles on the wear surface and then decreased as these particles leave the wear surface, leading to periodic fluctuations in the coefficient of friction. EDS analysis of the debris indicates that the wear resistance of composites with different Ti contents is superior to that of the high-speed steel friction pair. Therefore, it can be inferred that the coefficient of friction of high-speed steel falls within the range from 0.4 to 0.8.

AlCrFeNiTi$_{1.0}$-TiN coating and AlCrFeNiTi$_{1.5}$-TiN coating composites exhibit higher hardness based on the experiment results, demonstrating excellent wear resistance due to the presence of high-melting-point and high-heat-hardness TiN on composite surfaces and the precipitation of intermetallic compounds (σ phase and Ti$_3$Al phase). The resistance against the thermal softening is also improved, which implies that the local contact areas will have higher hardness to counteract

adhesive wear.

3 Conclusions

1) The crystal structure of $AlCrFeNiTi_x$ HEAs is primarily composed of B2 phase and A2 phase. The $AlCrFeNiTi_x$ HEA powders consist of agglomerates of nodular particles, and the elements are evenly distributed within the particles.

2) TiN content is increased with the increase in Ti content. In $AlCrFeNiTi_{1.5}$-TiN coating composite, the σ phase and Ti_3Al phase appear. With the increase in Ti content, the NiAl-rich B2 phase is transformed into the B2 phase of $AlNi_2Ti$, and the strength of the A2 phase is decreased.

3) The coated composites exhibit excellent hardness, and the hardness is significantly increased with the rise in Ti content. The maximum hardness of $AlCrFeNiTi_{1.5}$-TiN coating composite reaches 14 220 MPa. The wear resistance of the composite is significantly better than that of the reference SKH51 steel due to the formation of ceramic coating which contains the second phases (TiN) and TCP phases (σ phase, Ti_3Al phase). With the increase in Ti content, the wear mechanism changes from primary delamination wear with oxidative wear into pure delamination wear. The composites exhibit outstanding hardness and wear resistance.

4) The combined process of molten salt electro-deoxidation and cooperative hot-press sintering highlights the versatility of production in carbon steel-HEAs-ceramic coating composite materials under the conditions of short process and moderate temperatures. This process can also be used to synthesize high-entropy carbide-ceramic coatings. Furthermore, the carbon contamination and incomplete deoxidation during the electrochemical reduction process have negligible effects on the hardness and wear resistance of carbon steel-HEA-ceramic coating composite materials.

References

1 Garg R, Singh S K. *Environmental Science and Pollution Research*[J], 2022, 29(50): 75203

2 Wojciechowski J, Baraniak M, Lota G. *Ceramics International*[J], 2021, 47(17): 24770

3 Luo S, Zheng L, Luo H *et al*. *Applied Surface Science*[J], 2019, 486: 371

4 Koricherla M V, Torgerson T B, Alidokht S A *et al*. *Wear*[J], 2021, 476: 203746

5 Şap S, Uzun M, Usca Ü A *et al*. *Journal of Materials Research and Technology*[J], 2021, 15: 6990

6 Maodzeka D K, Olakanmi E O, Mosalagae M *et al*. *Optics & Laser Technology*[J], 2023, 159: 108914

7 Yu J K, Wang Y H, Zhao X C *et al*. *Advances in Materials Science and Engineering*[J], 2019, 2019: 2548285

8 Khademi A R, Afsari A. *Transactions of the Indian Institute of Metals*[J], 2017, 70: 1193

9 George E P, Raabe D, Ritchie R O. *Nature Reviews Materials*[J], 2019, 4(8): 515

10 Qiu Y, Thomas S, Gibson M A *et al*. *npj Materials Degradation*[J], 2017, 1(1): 15

11 Shi Y, Yang B, Liaw P K. *Metals*[J], 2017, 7(2): 43

12 Liu L Y, Zhang Y, Han J H *et al*. *Advanced Science*[J], 2021, 8(23): 2100870

13 Qin Cheng, Hou Hongmiao, Guo Ping *et al. Titanium Industry Progress*[J], 2023, 40(4): 44 (in Chinese)

14 Qi W J, Ding D S, Luo W J *et al*. *Coatings*[J], 2023, 13(7): 1246

15 Wang L M, Chen C C, Yeh J W *et al*. *Materials Chemistry and Physics*[J], 2011, 126(3): 880

16 Zhang X, Liu Y, Cheng H C *et al*. *Materials*[J], 2023, 16(14): 5059

17 Thawari N, Gullipalli C, Katiyar J K *et al*. *Materials Today Communications*[J], 2021, 28: 102604

18 Feng X G, Tang G Z, Sun M R *et al*. *Surface and Coatings Technology*[J], 2013, 228(S1): S424

19 Dolique V, Thomann A L, Brault P *et al*. *Materials Chemistry and Physics*[J], 2009, 117(1): 142

20 Wang J F, Bai S X, Ye Y C *et al*. *Rare Metals*[J], 2021, 40: 202

21 Zhou Z, Tao C F, Chen B *et al*. *Advanced Engineering Materials*[J], 2023, 25(12): 2201781

22 Yuan W, Li R, Chen Z *et al*. *Surface and Coatings Technology*[J], 2021, 405: 126582

23 Sure J, Vishnu D S M, Schwandt C. *Applied Materials Today*[J], 2017, 9: 111

24 Sure J, Vishnu D S M, Schwandt C. *Journal of Alloys and Compounds*[J], 2019, 776: 133

25 Wang B, Huang J, Fan J H *et al*. *Journal of the Electrochemical Society*[J], 2017, 164(14): E575

26 Jiao H D, Wang M Y, Tu J G *et al*. *Journal of the Electrochemical Society*[J], 2018, 165(11): D574

27 Chen G Z, Fray D J, Farthing T W. *Nature*[J], 2000, 407(6802): 361

28 Wang D, Jin X, Chen G Z. *Physical Chemistry*[J], 2008, 104: 189

29 Fray D J, Chen G Z. *Materials Science and Technology*[J], 2004, 20(3): 295

30 Lei Z F, Liu X J, Wu Y *et al*. *Nature*[J], 2018, 563(7732): 546

31 Wang Z, Baker I, Cai Z *et al*. *Acta Materialia*[J], 2016, 120: 228

32 Ge W J, Wu B, Wang S R *et al*. *Advanced Powder Technology*[J], 2017, 28(10): 2556

33 Tang Y, Wang S, Sun B *et al*. *Surface Review and Letters*[J], 2016, 23(4): 1650018

34 Ren M X, Wang G T, Li B S. *18th International Conference on Electronic Packaging Technology*[C]. Harbin: IEEE, 2017: 817

35 Dong Y, Lu Y P, Kong J R *et al*. *Journal of Alloys and*

Compounds[J], 2013, 573: 96
36 Sui Y W, Gao S, Chen X *et al*. *Vacuum*[J], 2017, 144: 80
37 Kang M, Lim K R, Won J W *et al*. *Journal of Alloys and Compounds*[J], 2018, 769: 808
38 Nong Z S, Lei Y N, Zhu J C. *Intermetallics*[J], 2018, 101: 144
39 Chuang M H, Tsai M H, Wang W R *et al*. *Acta Materialia*[J], 2011, 59(16): 6308
40 Khruschov M M. *Wear*[J], 1974, 28(1): 69
41 Farhat Z N. *Wear*[J], 2001, 250(1–12): 401

联合工艺制备钢表面高熵合金-陶瓷涂层复合材料及其力学性能

李 慧[1]，陈 庚[1]，张 胜[1]，梁精龙[1]，霍东兴[2]，杨 宇[3]
(1. 华北理工大学 冶金与能源学院 现代冶金技术教育部重点实验室，河北 唐山 063210)
(2. 华北理工大学 机械工程学院，河北 唐山 063210)
(3. 华北理工大学 综合测试分析中心，河北 唐山 063210)

摘 要：提出了一种制备低碳钢表面AlCrFeNiTi_x高熵合金-TiN陶瓷涂层复合材料的联合工艺（熔盐电脱氧+真空热压烧结），其中氮化物来自石墨模具和高熵合金粉末之间的BN隔离剂。探究了Ti含量对材料显微组织、极限抗拉伸强度、硬度和耐磨性能的影响，并对其结合机理进行了探究。结果表明，该复合材料具有优异的硬度和耐磨性能。随着Ti含量的增加，涂层复合材料的硬度显著提高。极高的耐磨性能是由于TiN的极高熔点和高热硬度能够有效防止磨损表面的氧化变形。

关键词：高熵合金；陶瓷涂层；熔盐电脱氧；真空热压烧结；力学性能

作者简介：李 慧，女，1981年生，博士，教授，华北理工大学冶金与能源学院现代冶金技术教育部重点实验室，河北 唐山 063210，E-mail：lh@ncst.edu.cn